

VIRTUAL SHIMMING AND MAGNETIC MEASUREMENTS OF TWO LONG PERIOD APPLE-II UNDULATORS AT THE CANADIAN LIGHT SOURCE

C. Baribeau[†], M. Sigrist, T. Pedersen, Canadian Light Source, University of Saskatchewan, 44 Innovation Boulevard, Saskatoon, Saskatchewan, S7N 2V3, Canada

Abstract

Assembly and shimming have completed for a pair of long period APPLE-II type elliptically polarized undulators, QP-EPU180 and EPU142, at the Canadian Light Source. Both devices were shimmed using a weighted cost single-objective simulated annealing algorithm, with shims generated iteratively based on Hall probe and flipping coil data. In this paper we present detailed measurements on the two EPUs, including their magnetic and spectral performance across a wide range of gap and polarization operating points, as well as measured and predicted changes in field due to the virtual shimming.

EPU SHIMMING AT CLS

QP-EPU180 is a quasiperiodic undulator sized to fill a straight section in the CLS storage ring. It is one half of a dual EPU previously reported on in [1]; the full D-EPU was installed in the CLS storage ring in spring 2017. EPU142 is one undulator sized to fill 1/2 a straight section. Final magnetic measurements of EPU142 concluded in fall 2018. Installation of EPU142 together with EPU54, which will occupy the same straight as EPU142 and the work for which is ongoing, is anticipated to occur in fall 2019.

The assembly of an EPU at the CLS begins with the installation of permanent magnet blocks onto the insertion device support structure, followed by precise positioning of each magnet to a reference zero position. The details of this work have been reported previously in [1].

An EPU is then optimized by virtual shimming. A shimming iteration consists of Hall probe (HP) and flipping coil (FC) measurements taken across multiple EPU operating modes; Table 1 lists the modes considered for EPU180. The measurement data are passed into a simulated annealing (SA) algorithm [2], which stochastically determines an optimal arrangement of virtual shims based on the figures of merit in Table 2.

Table 1: Modes Considered in QP-EPU180 Virtual Shimming

Polarization Mode	Gap [mm]	Girder Phases (G1, G2, G3, G4) [λ_{und}]			
Planar	15	0	0	0	0
Planar, 2 nd Gap	25	0	0	0	0
Vertical	15	-1/4	1/4	-1/4	1/4
Elliptical-Left	15	1/8	-1/8	1/8	-1/8
Elliptical-Right	15	-1/8	1/8	-1/8	1/8

[†] cameron.baribeau@lightsources.ca

The figures of merit are derived from HP and FC data and modified by shim signatures, i.e. predicted local changes in the field (integrals) due to displacing a given magnet by a discrete distance, e.g. 50 μ m. Shim signatures are calculated using a RADIA [3] model of the EPU. Weighting coefficients are applied to sum the figures of merit across operating modes and return a single “cost” for the algorithm to optimize.

Table 2: Figures of Merit Considered in Virtual Shimming Optimization of EPUs at CLS (coordinates: x-transverse horizontal; z-transverse vertical; s-longitudinal)

Figure of Merit	Derived From...	Typical Weight Factor
MAX $ \int Bds(x) $	FC	5
MAX $\int Bds(x) -$ MIN $\int Bds(x)$	FC	5
Integrated Multipoles	FC	Varies
MAX $\int Bds(s)$	HP	1
Exit $\iint Bdsds$	HP	1
RMS Phase Error	HP	3
Trajectory Straightness	HP	1

The SA algorithm is confined such that the solution of a shimming iteration will contain only up to 10-25 shims, which can feasibly be applied by 1-2 personnel in a matter of hours. Together with ~5 hours scanning time and ~8 hours of algorithm run time, it was possible to complete one virtual shimming iteration every 1-2 working days.

Once virtual shimming could no longer improve an EPU’s performance, a similar SA algorithm was employed for shimming with magic fingers (i.e. small end magnets for tuning field integrals). At this stage, figures of merit were restricted to transverse field integrals and multipole expansions thereof. Generally, best results were obtained by solving one longitudinal row of magic fingers at a time.

For QP-EPU180, the device was first assembled and shimmed as a periodic undulator and later modified for quasi-periodicity. After the modifications three virtual shim iterations were implemented, with no magic finger shimming.

Figure 1 shows the predicted and actual changes to EPU142 transverse field integrals (left) and beam trajectories (right) for a typical round of virtual shimming. While ~10 G·cm agreement with prediction was attainable for a single test shim, the ~20-40 G·cm accuracy seen in Fig. 1 was typical for multi-shim sets. In practice, accuracy

Content from this work may be used under the terms of the CC BY 3.0 licence (© 2019). Any distribution of this work must maintain attribution to the author(s), title of the work, publisher, and DOI

was limited more so by the physical positioning of the magnets rather than the predictive power of the model.

The overall agreement between prediction and measurement allowed for work on EPU142 to converge in just six virtual shimming iterations and one magic finger iteration. This is a large improvement over 22 virtual shim iterations for QP-EPU180 and 24 virtual shim iterations for EPU55. This improvement is largely thanks to resolving a scaling error in our handling of FC data, which was only identified after work competed on QP-EPU180.

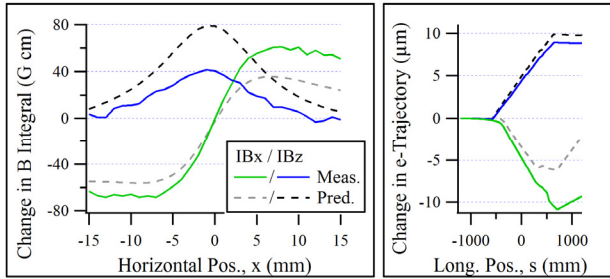


Figure 1: Measured and predicted changes to transverse field integrals (left) and exit trajectories (right) due to 10 virtual shims applied to EPU142 in shim iteration 5.

Figures 2 and 3 show normal and skew integrated multipoles, respectively, across all shimming iterations for QP-EPU180 and EPU142. Figure 4 shows beam trajectories for the same. For brevity, data are included for planar polarization mode only. However, note that the transverse field integral structure varies with polarization mode; magic finger shimming was used to balance the multipole structure between polarization extremes (i.e. planar horizontal and vertical modes).

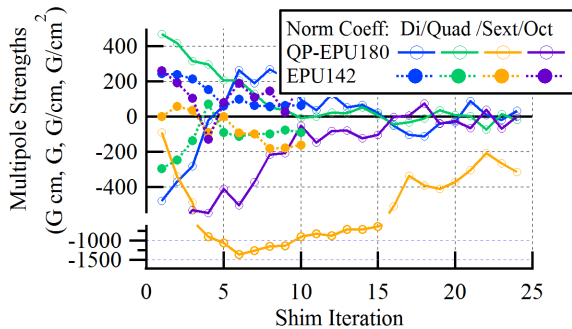


Figure 2: Normal multipole components throughout shimming QP-EPU180 and EPU142 (planar mode only).

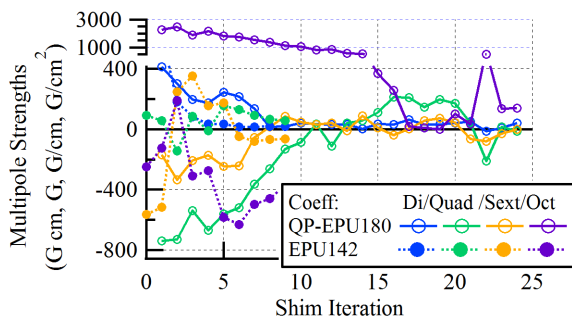


Figure 3: Skew multipole components throughout shimming QP-EPU180 and EPU142 (planar mode only).

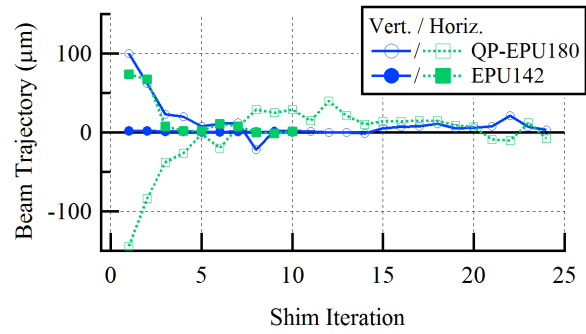


Figure 4: Exit trajectories throughout shimming QP-EPU180 and EPU142 (planar mode only).

IMPLEMENTING QUASI-PERIODICITY

QP-EPU180 was converted from a periodic device to a quasi-periodic one by displacing certain longitudinally polarized magnets (“H-blocks”) by a vertical offset δ . We follow the strategy put forward by Chavanne in [4], wherein the following sequence is used to determine which H-blocks are to be displaced:

$$x_k = k + \frac{1}{\eta - 1} \text{Floor}\left[\frac{k}{\eta + 1} + 1\right]$$

where the function “Floor[...]” rounds its argument down to the nearest integer and η is an inter-lattice ratio. For QP-EPU180, $\delta = 20$ mm and $\eta = \sqrt{5}$, which results in 12 positions across the device (i.e. 48 magnets total) to be modified. Figure 5 shows a series of undulator spectra derived from HP scans, each of which was taken between modifying 1 of the 12 sets of H-blocks. Spectra were calculated using the software package SRW [5] in IGOR Pro for a 6 mm \times 8 mm observation window 22 m downstream from the EPU. The gradual suppression of the periodic EPU’s peak at 8.5 eV and the development of the quasiperiodic peak at 10 eV agrees well with simulation.

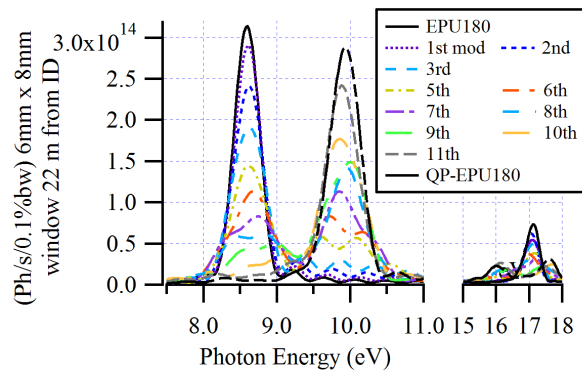


Figure 5: Undulator radiation at minimum gap planar mode calculated from Hall probe scans taken during incremental modification of EPU180 to implement quasi-periodicity.

Table 3 lists spectral intensities calculated from HP data for two polarization modes, normalized to the $n=1$ EPU180 periodic peak. The relative change in peak intensities when shifting from periodic (P) to quasiperiodic (QP) agrees with the magnetic design to within a few percent.

Table 3: EPU180 Undulator Harmonics Relative to the n=1 (Periodic) Peak for Planar and Vertical Polarizations

Undulator Harmonic, n	Planar		Vertical	
	P	QP	P	QP
1	1.00	0.94	1.00	1.04
2	0.23	0.10	0.22	0.24
3	0.73	0.06	1.05	0.56
4	0.48	0.02	0.71	0.25
5	0.58	0.06	0.78	0.17

MAGNETIC MEASUREMENTS

Final magnetic measurements spanned approximately two weeks of continuous scan time for each EPU. The final measurement set for QP-EPU180 consists of roughly 175 operating modes, which are summarized in Fig. 6. We report operating modes in terms of three degrees of freedom: the gap, and elliptical (Φ_E) and linear (Φ_L) phase parameters. The four EPU girder positions can be determined from Φ_E and Φ_L per the relations in Table 4.

Table 4: EPU Girder Positions Expressed in Terms of Elliptical and Linear Phase Parameters

Girder	Φ_E	$ \Phi_L (> 0)$	or	$ \Phi_L (< 0)$
1	$= \frac{1}{2} +$	1	+	0
2	$= -\frac{1}{2} +$	0	+	1
3	$= \frac{1}{2} -$	1	+	0
4	$= -\frac{1}{2} +$	0	-	1

For EPU142, we increased the number of scanned modes up to roughly 330. Figure 7 shows the polarization modes measured at minimum gap for EPU142 in terms of Φ_E and Φ_L . The wide coverage is to account for the fact that both devices require arbitrary polarization at the undulator in order to achieve circular light at the beamline end station; see [6] for further discussion.

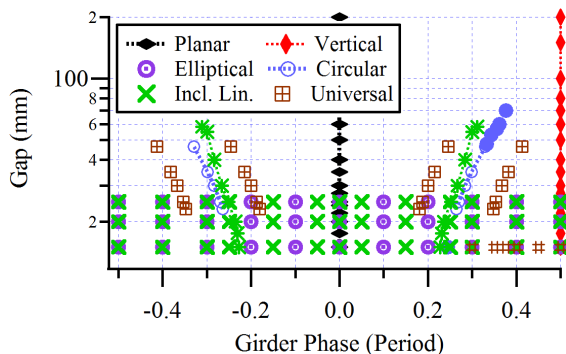


Figure 6: Gap and phase operating modes included in QP-EPU180 final magnetic measurements.

Figure 8 shows on-axis 1st field integrals for QP-EPU180 (top) and EPU142 (bottom). To avoid cluttering the data, we include only a representative subset of the measurements. The highlighted region at the left indicates data below each ID's low energy cut-off; horizontal red lines emphasize the design goals or double thereof. Both

devices cross into the region of 1-2 times the design goal for some modes, which is not ideal, but should be straightforward for correction coils to correct.

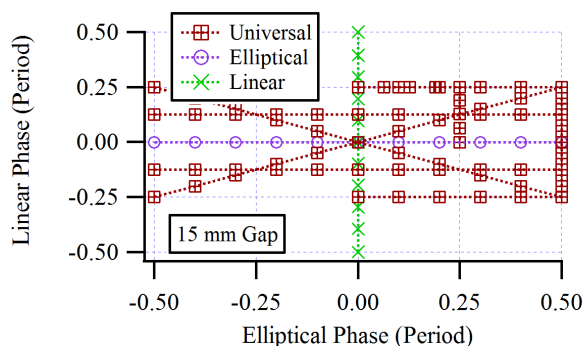


Figure 7: Polarization modes at minimum gap included in EPU142 final magnetic measurements.

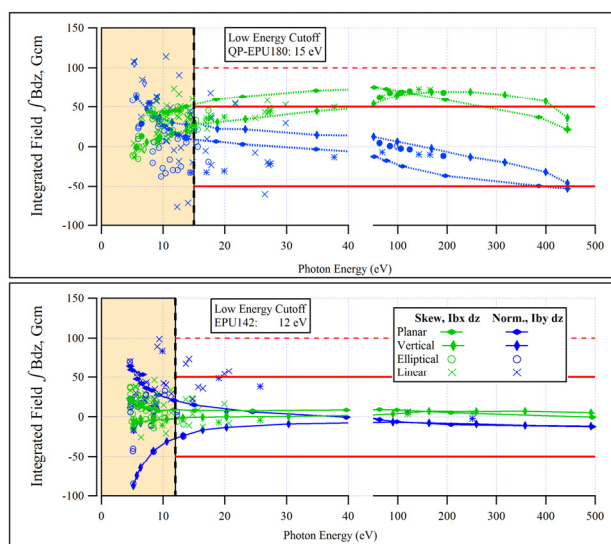


Figure 8: QP-EPU180 (top) & EPU142 (bottom) on-axis 1st field integrals against photon energy for select modes.

CONCLUSION

The CLS magnet mapping facility is actively producing APPLE-II type undulators for CLS beamlines. Workflow has been tuned in recent years and shimming of the latest EPU finished in less than half the time compared to one shimmed in 2016. Rigorous automated measurement has enabled the acquisition of a large data set showcasing the performance of multiple EPUs across hundreds of different operating modes.

REFERENCES

- [1] C. K. Baribeau, L. O. Dallin, J. M. Helfrich, T. M. Pedersen, M. J. Sigrist, and W. A. Wurtz, "Simulated and measured magnetic performance of a double APPLE-II undulator at the Canadian Light Source", in *Proc. IPAC'16*, Busan, Korea, May, pp. 4025-4027.
- [2] S. Kirkpatrick, C. D. Gelatt, M. P. Vecchi, "Optimization by Simulated Annealing", *Science New Series*, Vol. 220 (1983), pp. 671-680.

Content from this work may be used under the terms of the CC BY 3.0 licence (© 2019). Any distribution of this work must maintain attribution to the author(s), title of the work, publisher, and DOI

- [3] P. Elleaume, O. Chubar, and J. Chavanne, “Computing 3D magnetic fields from insertion devices”, in *proc. PAC97*, Vancouver, Canada, 1997, paper 9P027, pp. 3509-3511.
- [4] J. Chavanne, P. Elleaume, and P. Van Vaerenbergh, “Development of quasiperiodic undulators at the ESRF”, in *Proc. EPAC'98*, Stockholm, Sweden, 1998, paper MOP07F, pp. 2213-2215.
- [5] O. Chubar and P. Elleaume, “Accurate and Efficient Computation of Synchrotron Radiation in the Near Field Region”, in *proc. EPAC'98*, Stockholm, Sweden, Jun. 1998, paper THP01G, pp. 1177-1179.
- [6] M. J. Sigrist, C. K. Baribeau, and T. M. Pedersen, “Arbitrary Photon Polarisation Modelling of APPLE-II EPU’s”, in *Proc. IPAC'19*, Melbourne, Australia, May 2019, paper TUPRB005, this conference.